Topological Characterization of Nanoporous Gold during Coarsening

by

Ryan Rosario

Submitted to the Department of Materials Science and Engineering in Partial Fulfillment of the Requirements for the Degree of

Bachelor of Science

at the

Massachusetts Institute of Technology

June 2012

Signature of Author:_____
Department of Materials Science and Engineering
May 14, 2012

Certified by:_____
Michael J. Demkowicz
Assistant Professor of Materials Science and Engineering
Thesis Supervisor

Accepted by:_____
Jeffrey C. Grossman
Professor of Materials Science and Engineering
Chair, Undergraduate Committee

Topological Characterization of Nanoporous Gold during Coarsening

by

Ryan Rosario

Submitted to the Department of Materials Science
and Engineering on May 14, 2012 in Partial Fulfillment
of the Requirements for the Degree of Bachelor of Science
in Materials Science and Engineering

ABSTRACT

Previous studies of nanoporous gold have found that, during the coarsening process, the genus per characteristic volume of nanoporous gold has remained constant. Using a rolling-ball type algorithm, in which a test probe rolls over the surface to identify atoms, several test structures and a small-scale nanoporous structure were meshed. The genus was then calculated for each of these meshed structures. It was found that an algorithm that accounts for periodic boundary conditions is required for an accurate genus calculation.

Thesis Supervisor: Michael J. Demkowicz
Title: Assistant Professor of Materials Science and Engineering

Table of Contents

1. INTRODUCTION

1.1. Brief Overview Of Nanoporous Metals

Techniques for creating nanoporous metals have been known for centuries. Known by goldsmiths as depletion gilding, the technique was mainly used to create a nearly pure gold surface from a less expensive gold alloy. Early Andean goldsmiths used the technique to created patterned surfaces on the pieces they created[i]. In the medieval Europe, jewelry makers would create nanoporous sheets of precious metals out of impure sheets[1]. Nanoporous metals are predominantly created by a technique known as dealloying, where a less noble metal from an alloy is selectively dissolved by an electrolyte solution. This dealloying process leaves behind a nanoporous network of ligaments that is mostly made of the more noble metal[iii]. This technique has been used to create nanoporous structures of a variety of metals, most notably gold, platinum, and copper[iv,v,vi,vii]. The phenomenon is also observed in the corrosion of several commonly used alloy systems, namely brass, stainless steel, and Cu-Al alloys[1,viii,ix].

Figure 1. Body plaque from an early Andean cemetery in Panama. Golden appearance was enhanced by depletion gilding[2].

Nanoporous metals created by dealloying of alloys with a more noble metal concentration above a certain threshold are found to have bicontinuous structures, where the unbroken networks of high purity ligaments and pores completely interpenetrate[x,xi]. Above this threshold, the pore networks do not interconnect and the less noble metal dissolves much less[10]. The pore and void networks created by dealloying have characteristic lengths on the order of 1-100nm. Although having dimensions of this order technically makes the dealloyed structures mesoporous materials, which have pore size greater than 2nm and less than 50nm, or macroporous, which have a pore size greater than 50nm, dealloyed structures are referred to as nanoporous materials due to the wide variety of phenomena that are observed in materials with nanometer-scale dimensions[xii].

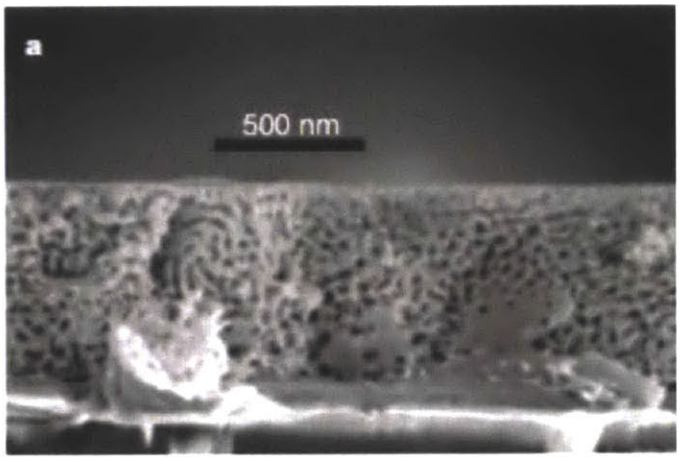

Figure 2. Scanning electron micrographs of nanoporous gold made from the selective dealloying of an Ag-Au alloy[4].

These nanoporous metal networks were found to have a variety of desirable properties that make them suitable for wide variety of potential applications. Like many materials with dimensions in the nanometer regime, nanoporous metals were found to have a very strong surface plasmon resonance effect, which makes them very interesting for numerous sensing applications[xiii]. While few studies document

how this property could be utilized in sensors made of np-Au, numerous studies document its effect in gold nanoparticles[xiv].

Nanoporous metals have an extremely high surface area, which makes them attractive for many applications, such as electrodes, catalysts, and sensors. In a study by K. Hu et al., a sensor system, comprised of gold nanoparticles coupled to reporter DNA anchored to a np-Au electrode, showed a drastically increased sensitivity and sensitivity[xv]. R.G. Mitsunori Hieda et al. increased the sensitivity of a quartz crystal microbalance, which are useful in a wide range of sensing applications, by replacing the traditional electrode with a np-Au[xvi]. Many studies report drastically increased mass activity for nanoporous metal catalysts, due mainly to a higher active area[xvii,xviii,xix,xx]. Np-Au was found to have a measureable surface-chemistry-driven actuation, due to the high surface area available for adsorption[xxi].

Nanoporous metals were found to have very high strengths, similar to the theoretical strength of gold, despite being very porous[xxii,xxiii,xxiv]. The high strength observed in nanoporous metals was explained by dislocation starvation, which occurs when

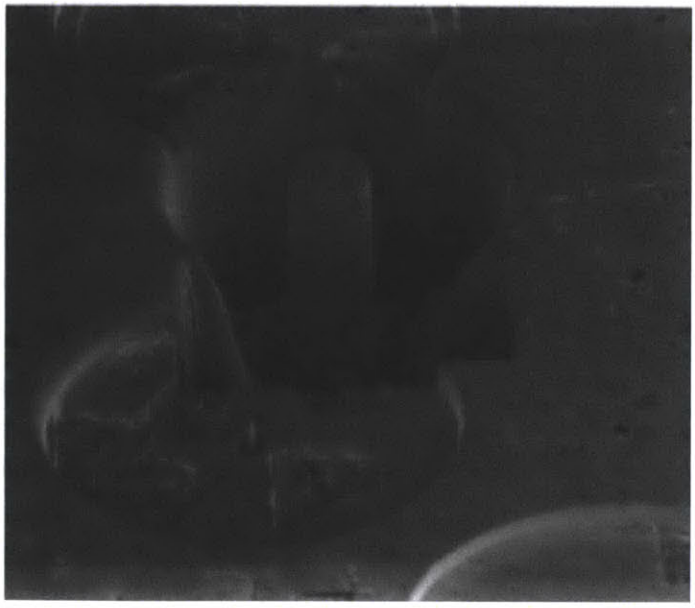

Figure 3. Gold nanopillar used in mechanical study of metals with nanometer-scale dimensions. Found that strength approached theoretical limit due to dislocation starving[23].

the ligament radius is below a critical radius [23,24]. This makes nanoporous metal foams very attractive for applications requiring both lightweight and high strength. Due to it numerous desirable properties and potential applications, uncovering the mechanism by which nanoporous metals develop and identifying key differences in structure is particularly important.

1.2. Nanoporous Metal Morphology

Nanoporous metal foams have a complicated morphology that is normally described by a variety of geometric and topological parameters. Nanoporous metal foams are always open-cell foams, that is to say that the pores form an interconnected network[10,11]. While nanoporous metals are sometimes described as foams, their structure is distinctly different from foams. Nanoporous metals can have many more ligaments connecting at a single node than what is typically observed in foams[xxv]. Nanoporous metals also have different topological properties, namely they may have rings present in the middle of ligaments[25].

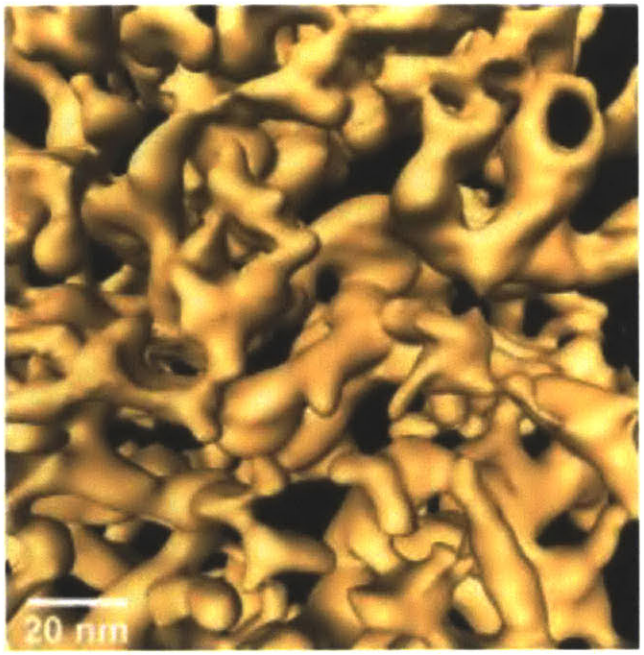

Figure 4. Nanoporous gold structure, digitally reconstructed from transmission electron micrographs. Not the rings present in ligaments[25].

Interestingly, nanoporous metals maintain the crystallinity of their native crystal after dealloying, though the resultant structure is highly strained[xxvi]. This means that crystal domains can exist that are much larger than the characteristic dimensions of the nanoporous structure, which has interesting ramifications for the properties of the material[25].

Nanoporous metals have a wide distribution of ligament and pore sizes, which can have drastic effects on the properties of the material. In a study by Rosner et al., nanoporous metal samples were digitally reconstructed from topological mappings produced using transmission electron tomography. They found that there is a very wide distribution in ligament in pore sizes[25]. As a result of this wide distribution, estimates of specific surface area, a very critical property for many sensing applications, cannot rely on the average size of ligaments and pores, as these estimates may be very incorrect[25]. This study also revealed the presence of enclosed bubbles within the

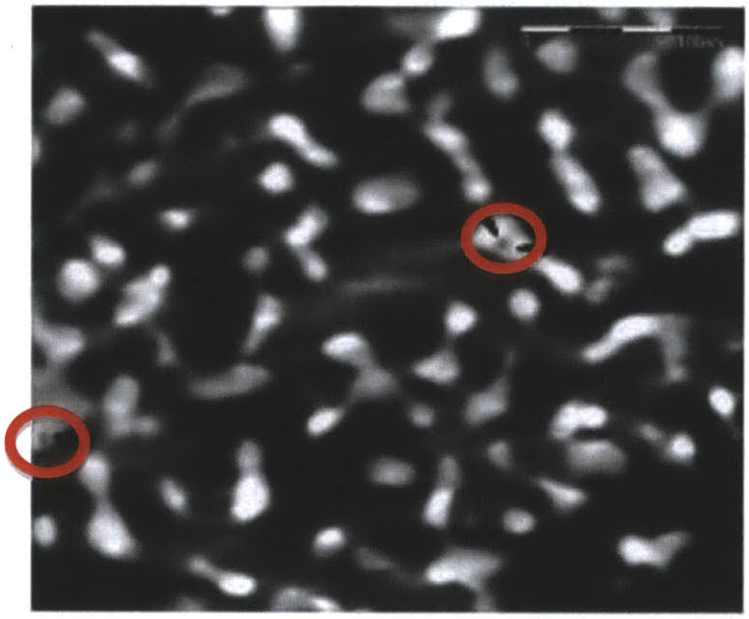

Figure 5. Image from transmission electron micrograph depicting enclosed bubbles in ligaments[25].

nanoporous metal structure, which has interesting ramifications for the mechanism by which coarsening proceeds, which will be discussed later[25].

Both the topological genus and the surface curvature of nanoporous metals are two properties, which are closely connected with explanations for the coarsening mechanism of nanoporous metals. While few experimental studies examine the genus of nanoporous metals, many computational studies look into the time evolution of the topological genus. In a study by Kwon et al., it was noted that the characteristic genus of bicontinuous structures simulated using finite difference analysis was time invariant, which would be interesting to confirm via molecular dynamics simulations[xxvii]. For surface curvatures, some studies have found a zero net curvature for samples at equilibrium, while other studies have found positive mean curvatures[26,xxviii].

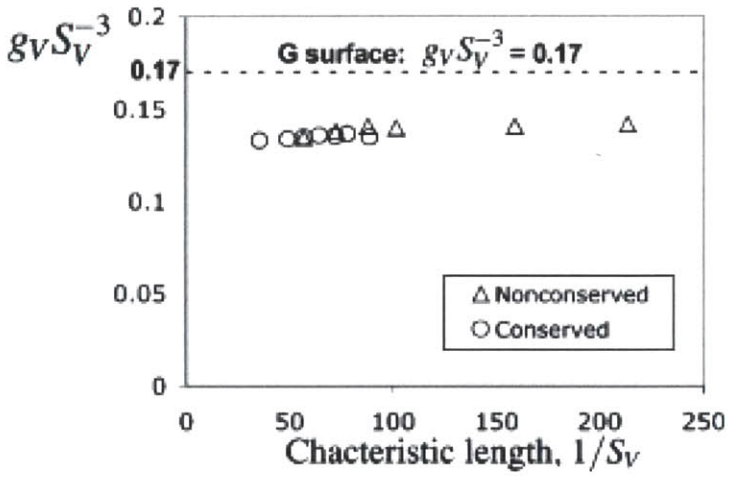

Figure 6. Genus per characteristic volume vs. characteristic length for simulations from Kwon et al. Since characteristic length varies with time, this also shows time evolution of genus per characteristic volume. Not how the quantity is constant[27].

1.3. Theories for the Structural Evolution of Nanoporous Gold

Despite the fact that nanoporous metals have been known to exist for decades, little work was done to investigate the mechanism by which the

nanoporous network forms until the early 2000's. Several studies noted the morphology of alloys during the early stages of dealloying, namely the fact that small islands of the more noble metal formed on the surface of the alloys, but they could only conjecture at the underlying mechanisms by which those morphologies evolved, due to the lack of equipment with the necessary spatio-temporal resolution for experiments[xxix]. More recent studies, which rely primarily on simulation, have attempted to identify the mechanism by which these nanoporous structures form. Two potential theories have arisen due to these computational studies: one based on surface-diffusion and one based on local plasticity in the material.

1.3.1. Surface-Diffusion-Based Theory for Porosity Evolution and Coarsening

The most widely accepted model for the evolution of nanoporous materials is based on the diffusion of gold surface atoms during the dissolution process. Herring originally mentioned this theory, but he was unable to prove his hypothesis, due to the lack of the necessary computational or experimental capabilities[xxx]. Erlebacher et al. supported a surface-diffusion-based hypothesis and proposed a mechanism to explain the structural evolution of nanoporous metals.

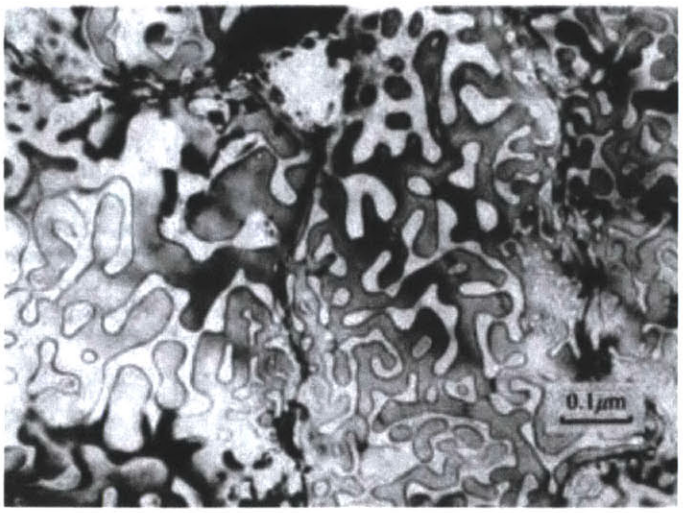

Figure 7. Transmission electron micrograph of gold islands formed during early stages of dealloying of an Ag-Au alloy[29].

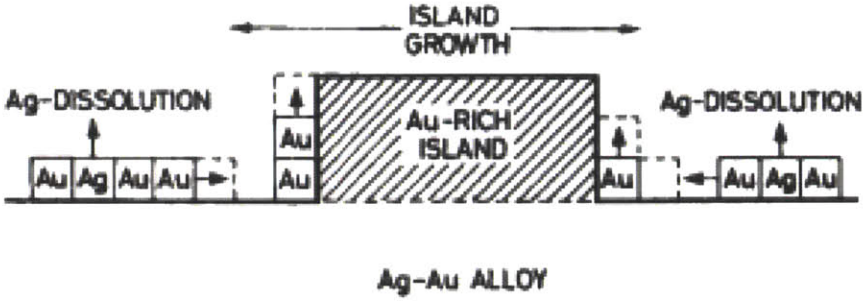

Figure 8. Schematic of the mechanism by which gold-rich clusters form during the dissolution of silver from an Ag-Au alloy. The mechanism was originally proposed by Forty in the late 1970's, but he lacked the proper computational or experimental capabilities to observe the mechanism[29].

To explain the formation of these nanoporous structures during dissolution, Erlebacher et al. used Ag-Au as a representative alloy. Starting with the bulk material, the electrolyte solution selectively dissolved the silver atoms, leaving behind a layer of gold atoms[3]. At this solid-electrolyte boundary, the gold adatoms have an extremely low solubility, on the order of 10^{-7}, which results in a rapid, spontaneous phase separation of the system into an island of gold atoms and the electrolyte solution[4]. This phase separation occurs so rapidly because the gold adatom concentration at the interface lies in the spinodal region of the solubility curve[3]. The separation results in a passivated gold-rich surface and a native alloy surface exposed to the electrolyte solution[4]. Silver atoms in the exposed native alloy will then dissolve, and the process continues[4]. As more and more layers are exposed to the electrolyte solution, the spinodal decomposition of the gold adatoms occurs on an increasingly non-uniform surface, which, after complete dealloying, will result in a nanoporous structure[4]. Kinetic Monte Carlo simulations using this surface-diffusion-based mechanism have produced nanoporous structures that resemble

the np-Au produced experimentally[4]. The computational model discounted the notion that diffusion through the bulk of the material could produce the nanoporous structure, because bulk diffusion occurs at too long of a time-scale to produce nanoporous structures created experimentally[4].

While a surface-diffusion-based model can adequately explain structural evolution during the dissolution process, there are several key criticisms of a surface-diffusion-based model for coarsening, due to disparities between the models and experimental evidence. For an on-lattice surface diffusion model, the number of lattice sites, and thus the volume of the sample, would remain constant; therefore there would be no volume change during dealloying. However, experimentally produced nanoporous metals report a volume change of up to 30%[xxxi]. For a model based *only* on surface diffusion, enclosed voids would not form, but voids have been observed experimentally[25]. Lastly, a surface-diffusion-based model would predict that high curvature regions would quickly smooth out, because curvature is big driving force in surface diffusion. However, high curvature regions associated with ligament pinch-off have been observed in np-Au samples[xxxii].

Figure 9. Nanoporous gold created through kinetic Monte Carlo simulation[4].

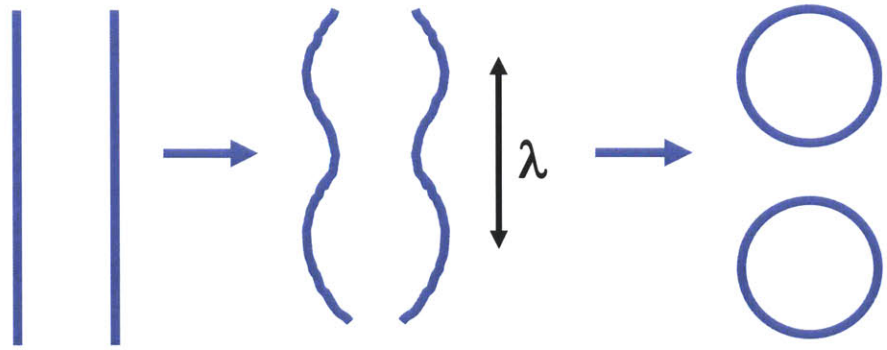

Figure 10. Cartoon illustrating the effect of Rayleigh instabilities. If some unstable surface is subject to some deformation of wavelength λ, then the amplitude of the deformation will spontaneously increase until separate bubbles are formed, due to the reduction in surface energy of the system.

To explain the presence of enclosed voids and high curvature regions, Erlebacher et al. proposed a new surface-diffusion-based model, which accounts for the presence of enclosed voids and high-curvature regions by accounting for the effects of Rayleigh instabilities on the structural evolution of nanoporous metals. Previously, surface-diffusion based models only examined driving forces associated with smoothing out high-curvature regions[33]. They did not account for the pulling away of material from saddle-point curvature ligaments[xxxiii]. At these saddle-point type nodes, material will gradually pull away from the node until pinch-off occurs[33]. The kinetics of this pulling-away are controlled by Rayleigh type instabilities[33]. In a Rayleigh-type instability, a structure, classically a cylinder, perturbed by some critical wavelength, λ_{crit}, will cause the structure to break up into a series of droplets, due to the effect of reducing the overall surface energy of the system. Applied to np-Au, Rayleigh-type instabilities can cause either ligament pinch-off or void formation[32]. This type of coarsening will result in the effect of reducing the effect of the topological genus for the observed system.

1.3.3. Plasticity-Based Theory of Coarsening

Plasticity-based theories for the structural evolution attempt to explain the presence of enclosed voids and ligament pinch-off with local plasticity that occurs at nodes. Kolluri et al. used MD simulations to show that local plasticity at nodes can cause the collapse of ligaments onto nearby ligaments[xxxiv]. Dislocation glide across the ligament cross-section causes ligament pinch-off, which is then immediately followed by the collapse onto adjacent ligaments[34]. For spontaneous coarsening, the reduction in surface energy compensates for the plastic work done by this network restructuring[34]. This implies that there is a critical radius for a stable ligament[34]. This theory of coarsening does not necessarily oppose the surface-diffusion-based theory for coarsening proposed by Erlebacher et al., because both can occur simultaneously within a nanoporous structure[34]. This type of coarsening, like that proposed by Erlebacher et al., will result in the effect of reducing the effect of the topological genus for the observed system.

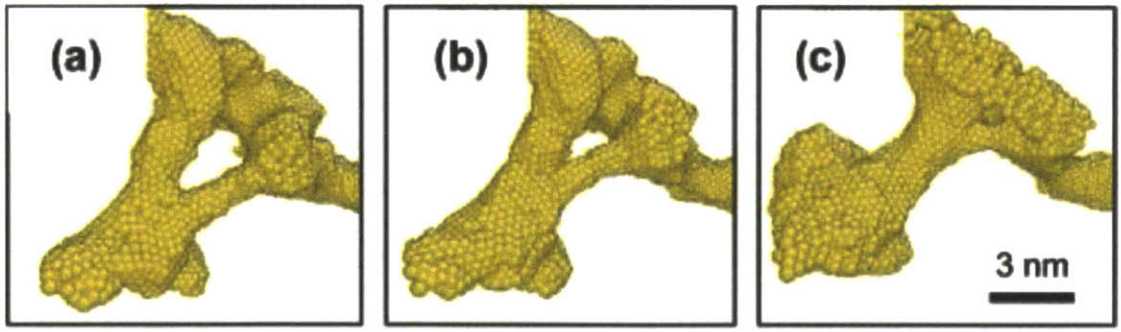

Figure 11. Successive images depicting a ligament collapse event in an MD simulation. This collapse event is enabled by dislocation glide within the ligaments[35].

1.4. MD Overview and Creation of Nanoporous Structures

The nanoporous structures examined in this study were created through a combination of conjugate gradient potential energy minimization (PEM) and molecular dynamics (MD) simulations. To create the initial structure, points on an evenly distributed lattice were subject to some random displacement. The total potential energy of the system was then minimized by moving the atoms in the opposite direction of the spatial gradient of potential energy, which was calculated using an embedded atom potential for gold. The result was a foam-like structure[34]. This structure was then relaxed at constant temperature and atomic motions during coarsening were modeled using MD simulations.

In layman's terms, an MD simulation finds the force on each atom based on the positions of other atoms in a structure. The calculated forces, along with the velocity and the current position of the atoms, are then used to calculate new position of the atoms after some designated time step. In order to calculate the forces on the atoms, an inputted potential must be used. Many different types of potentials exist, but for metallic systems, embedded

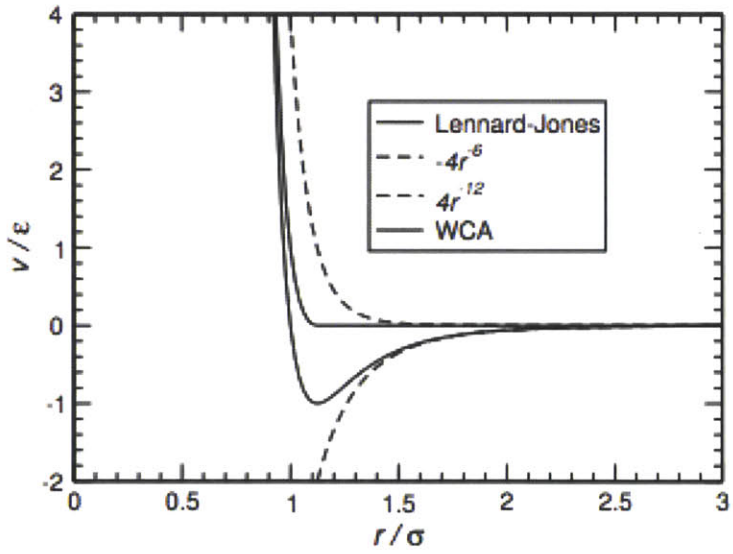

Figure 12. Simple Lennard-Jones pair potential used in early MD simulations to calculate forces acting on atoms[37].

atom method (EAM) potentials are most commonly used, due to their success in predicting physical behavior. EAM potentials have the following basic form:

$$E_{tot} = \sum_i F_i(\rho_i(R_i)) + \frac{1}{2}\sum_{i,j} \phi(R_{i,j}) \qquad (1)$$

where E_{tot} is the total potential energy, ρ_i is the electron density of the system without the at position $R_{i,}$, and ϕ is an electrostatic pair potential[xxxv]. Once the energy of the system is calculated, the derivative of the energy can then be taken to find force, one can solve Newtown's equations of motion to find position. For a more detailed introduction to MD simulation, can be found in Ref. 36.

2. GENUS AND CURVATURE

The main focus of this study is to examine the topological genus and curvature of nanoporous structures over time. As such, a detailed explanation of both genus and curvature and how each is calculated using a point cloud is required to understand the findings of this study.

2.1. Genus

Before strictly defining genus, it is helpful to review some of the basic concepts of topology that are relevant to this investigation. In his investigation of polyhedra, Euler discovered an interesting invariant of all convex polyhedra:

$$N - E + F = 2 \qquad (2)$$

where N is the number of vertices, E is the number of edges, and F is the number of faces. In order to illustrate this concept, some sample figures are depicted in Figure

Table 1. Lists the number of vertices (N), edges (E), and face (F) of some sample surfaces of increasing complexity. As is shown in the last column for the given examples, the quantity N-E-F is 2 for all polyhedra.

Shape	N	E	F	N-E+F
Square Pyramid	5	8	5	2
Cube	8	12	6	2
Hexagonal Prism	12	18	8	2
Dodecahedron	20	30	12	2

13 with the corresponding values for N, E, and F in table 1. As you can plainly see in each of the test cases, Euler's theorem holds. This idea, that an invariant quantity exists that links different features of different features helped to spawn some of the key ideas that led to the field of modern topology. When the quantity in equation 2 was extended to all polyhedra, the quantity known as the Euler characteristic was developed:

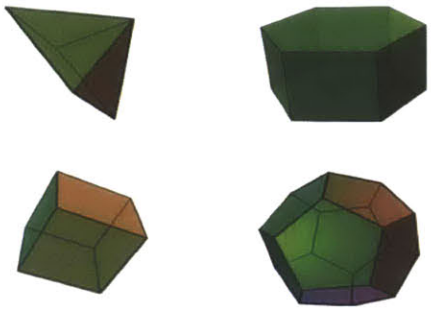

Figure 13. Depictions of some common polyhedra.

$$N - E + F = \chi \tag{3}$$

where χ is the Euler characteristic for a surface. The Euler characteristic is what is known as a topological invariant. That is to say, regardless of the way in which one partitions a surface into faces, the resulting Euler characteristic will always be the same. The Euler characteristic will also be identical for homeomorphic surfaces.

Rather than give a strict definition of homeomorphism, which requires advanced topology concepts outside the required understanding for this study, I will give some simple examples that illustrate the concept of homeomorphism. First, let us consider all the shapes presented in Figure 13. If all of the shapes were made of some moldable rubber, one could stretch any one starting shape into any other shape. All of these shapes are homeomorphic to each other. Second, consider the surfaces presented in Figure 14. All of these surfaces are also homeomorphic to each other, because they can be deformed into one another. However, the surfaces in Figure 13 are not homeomorphic to those in Figure 14, because the surfaces in Figure 13 cannot be deformed into the surfaces in Figure 14 without cutting or sticking together two of the surfaces. It is important to note that, while two shapes that can be deformed into the other are homeomorphic, this is not required for homeomorphism. For two shapes to be homeomorphic, they only need a continuous mapping and a continuous inverse. This basic idea of homeomorphism will help in the comprehension of the idea of topological genus.

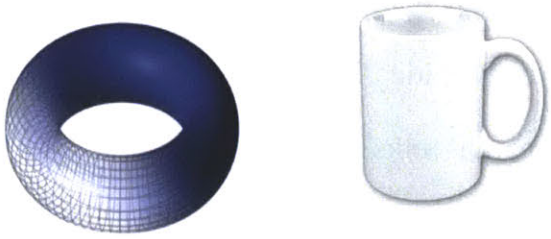

Figure 14. Two homeomorphic shapes, each of which can be deformed to form the other, though this is not require for homeomorphism.

The topological genus is defined as the number of handles that a surface has, or alternatively, as the maximum number of cuts one can make in a surface without

dividing the surface into two distinct pieces. In order to calculate the genus of a surface, one can use the Poincare formula:

$$N - E + F = 2 - 2g \tag{4}$$

where *g* is the topological genus, and the quantity *2-2g* is the Euler characteristic for a surface. This definition of genus stems from the concept of the Euler characteristic. Starting with any convex polyhedron, the Euler characteristic for that surface is two. For every handle that one adds to the surface of that polyhedron, the overall Euler characteristic will be reduced by two. One can then deform that polyhedron with handles into other homeomorphic shapes. Some representative shapes and their corresponding genus are depicted in Figure 15. Applying this concept to nanoporous metals, one could start with a sphere and add handles onto its surface to create a shape that is homeomorphic to a nanoporous metal. Since all the surfaces used in this study are comprised of triangulated meshes, the Poincare formula can be further modified to simplify calculation:

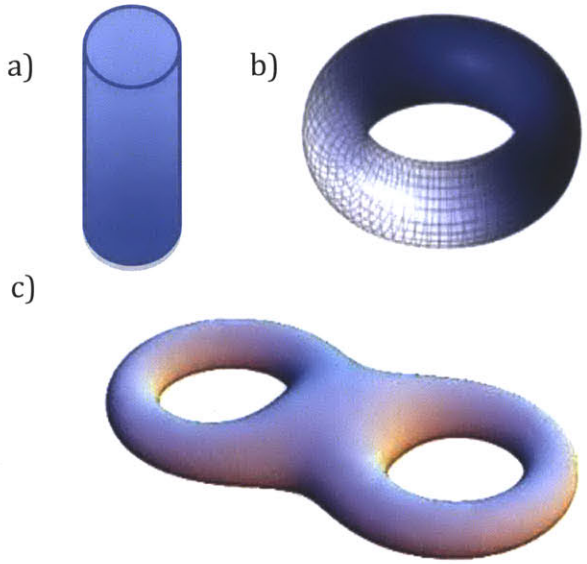

Figure 15. Three different shapes with three different genera. Shape (a) has a genus of zero, (b) a genus of one, and (c) a genus of two.

$$N - \frac{1}{2}F = 2 - 2g \tag{5}$$

This relationship arises from the face that every face has three edges, and that every edge is shared by two triangles.

Equation 2 only holds for hollow surfaces, that is surfaces without any interior. For every interior surface, which in the case of nanoporous metals would be an enclosed bubble in a ligament, the overall topological genus is reduced by one. This gives another alternative definition for the genus of surfaces:

$$g = n_h - n_b \tag{6}$$

where n_h is the number of hole, and n_b is the number of bubbles[xxxvii]. In terms of the Euler characteristic, one could think that each disconnected polyhedron has an Euler characteristic of two, and each handle on each of those polyhedra reduces the overall Euler characteristic of the system by two. For a more comprehensive introduction to topology, see Ref. 38.

2.2. Meshing Surfaces

In order to apply a triangulated mesh to the surfaces, the by L.M. Dupuy and R.E. Rudd was implemented in MATLAB[xxxix]. This algorithm is similar to that used for finding the r-reduced surface of biological molecules in simulation[39]. Conceptually, the algorithm identifies surface triangles by rolling a test probe across a surface. Whenever the test probe touches three atoms simultaneously, it creates a surface triangle using those three atoms as the vertices of the triangle.

In order to create a surface mesh, the first challenge is to identify the first triangle of the mesh. In the paper by Dupuy and Rudd, they suggest a method for completely automating the location of the first triangle; however, in order to reduce the challenge of coding the algorithm in MATLAB, one of the atoms of the first triangle was found manually using the AtomEye visualization package. Once the first atom is selected, the atoms that form the first surface triangle must satisfy two criteria: 1) the atoms must be sufficiently exposed to form a surface element with all three atoms in contact with the probe sphere, and 2) there must be no atoms within R_{tot}, which is the sum of the atomic radius and radius of the test probe used to tessellate the surface.

The first criterion can be confirmed with several mathematical relations. To properly orient the first triangle, and all subsequent triangles, a point outside of the surface is given. A properly oriented first triangle satisfies the following relation:

$$AS_0 \cdot (AB \times AC) > 0 \tag{7}$$

where A, B, and C are the locations of the atoms being tested, and S_0 is the position of the point outside of the surface. It is important to note that, for nanoporous structures the segment AS_0 must not pass through the surface. Once the surface element is properly oriented, one must then confirm that the circumscribed triangle of the three points has a radius less then R_{tot}:

$$R_{tot} > R_c = \frac{ABACBC}{2||AB \times AC||} \tag{8}$$

where R_c is the radius of the circle circumscribed about atoms A, B, and C. Once atoms A, B, and C have passed this test, the circumcenter of the circumscribed triangle is then found:

$$AG = \frac{(AB^2 - AB \cdot AC)AC^2AB + (AC^2 - AB \cdot AC)AB^2AC}{2||AB \times AC||^2} \quad (9)$$

where AG is the segment connecting atom A and the circumcenter G. Once this position is found, the position of the test probe relative to the surface can be calculated:

$$h = \sqrt{R_{tot}^2 - R_c^2} \quad (10)$$

$$AS = AG + h\frac{AB \times AC}{||AB \times AC||} \quad (11)$$

where h is the distance between the test probe, S, and G. Once S is known, criterion two can be confirmed by calculating the distance between S and all other nearby atoms. After the initial triangle is found, all other surface triangles can then be found.

All other atoms within $2R_{tot}$ of A and B of the initial triangle were then calculated. These atoms were stored as potential points for the third vertex of the next surface triangle, where A and B are the other two vertices. The position of the test probe is then calculated for each of the potential triplets of atoms as detailed above. The rotation angle of the probe sphere about BC is then calculated:

$$\cos\alpha'' = \frac{HS \cdot HS''}{HS\, HS''} \tag{12}$$

$$\sin\alpha'' = \frac{(HS \times HS'') \cdot AB}{HS\, HS''\, AB} \tag{13}$$

where α'' is the rotation angle, H is the midpoint of the segment AB, and S'' is the position of the test probe for the new triplet. The point that minimizes this rotation angle α'' is then selected as the third vertex for the new surface triangle. This process is then repeated for all found segments until no new surface elements are identified. In order to prevent the repeated storage of the same surface element, measures are taken. First, each segment is stored with the position of the test probe that was used to identify the segment. Second, once each segment is used to identify a surface element, it is flagged as used.

2.3. Meshing with Periodic Boundary Conditions

In order to simulate a bulk material, many simulations rely on the usage of periodic boundary conditions (PBC's). PBC's mimic the behavior of bulk material in a clever way. The atoms near a periodic boundary influence the motion of atoms at the opposite corresponding boundary. For example, if there is a simulation cell of dimensions L_x, L_y, and L_z, then an atom at (x_0, y_0, z_0) will feel a force from an atom at position $(x_0, y_0, L_z - z_0)$ as if it were $2z_0$ away. If an atom were to undergo a displacement that would cause it to pass through a periodic boundary, then that atom will appear at the opposite side of the simulation cell. That is to say, if an atom at position (x_0, y_0, z_0) were to undergo a displacement that would move it to a new

position (x_0, y_0, $-z_0$), then it would appear at the position (x_0, y_0, $L-z_0$) in the simulation cell.

PBC's pose a problem for meshing because, while atoms near a periodic boundary may seem to be at a surface according to the position data in the simulation file, they may have neighbors that lie across the periodic boundary. If these atoms at the boundary were considered surface atoms rather than in contact with the atoms across the periodic boundary, then the overall calculated genus could be less than the actual genus for the observed volume. Figure 16 clearly illustrates this point. In order to allow the meshing program to account for PBC's, a simple distance minimization was performed.

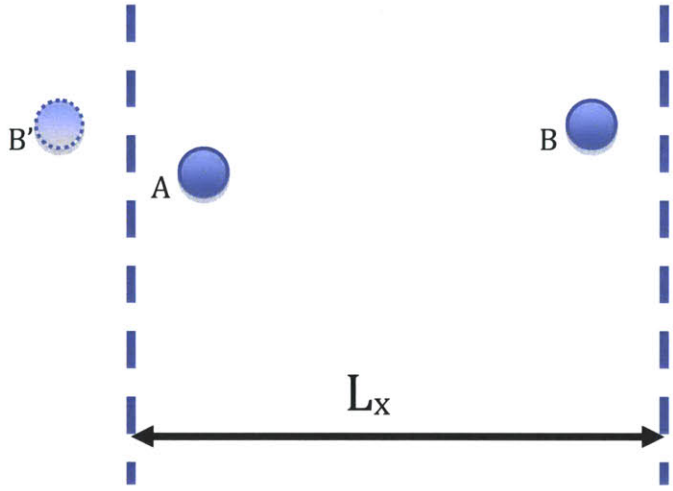

Figure 16. Cartoon illustrating the effect of PBC's. The dashed lines are periodic boundaries. Note how atom A feels a force from atom B as if atom B were in position B'.

According to PBC's, for every atom in a simulation cell, a virtual atom exists at periodic intervals in each direction. For an atom at (x_0, y_0, z_0), a virtual atom exists at (x_0+mL_x, y_0+nL_y, z_0+oL_z), where m, n, and o are integers, and L_x, L_y, and L_z are the dimensions of the simulation cell. In order to find the minimum distance between any two atoms being examined in the meshing function, then the simulation cell

length can be added or subtracted to each dimension, and the minimum point corresponding to the minimum distance found by adjusting the positions by the simulation cell lengths can be used for calculation. This will allow the meshing algorithm to jump across periodic boundaries. It is important that, when data is stored about each of the segments, the data for the atoms in their original positions are used, to allow all checks to function properly. All code used for analysis of structures is given in Appendix A.

3. RESULTS AND DISCUSSION

3.1. Simple Test Cases

Several meshing techniques were attempted before settling on the use of the meshing algorithm described previously. In order validate the meshing technique used in this study a variety of simple test structures were used, for which the value for genus was already known. In order for the code to pass the validation, the outputted mesh needed to yield the correct value for genus when the appropriate values for the number of vertices and the number of faces were inputted into Equation 5.

The first and most simple test structure used was a cube with points on a cubic lattice. Each point in the cubic lattice was subject to some random displacement. This random displacement was included in order to prevent the existence of degenerate surface elements. A degenerate surface element is one where the test probe simultaneously touches four or more atoms. Using the above algorithm, the resultant mesh would have intersecting surface elements if a degenerate surface element were encountered, which would result in an incorrect

value for the calculated genus. Such degenerate surface elements are exceedingly uncommon in simulation, as such they were not accounted for when implementing the algorithm describe above.

For the test structure, lattice points were approximately 0.1 units apart, with each side having a total length of 1 unit. The points on the lattice were subject to a random displacement in each direction of (0,0.001]. Using the Dupuy and Rudd algorithm with an atomic radius of 0.048 units and a test probe radius equal to the atomic radius, a mesh with 602 vertices and 1200 faces was produced. The Dupuy and Rudd algorithm successfully identified all the surface points for the test structure, which was one validation of its efficacy. Using values for the number of vertices and faces of the surface mesh, the calculated genus for the surface was found to be zero, which matched the known value. An atomic view of the cubic test structure and the mesh produced when using the Dupuy and Rudd algorithm are given in Figure MM. When using this test structure, the convex hull of a mesh created using the Delaunay triangulation method within MATLAB was also used, which also produced the correct value for genus and successfully identified all surface points.

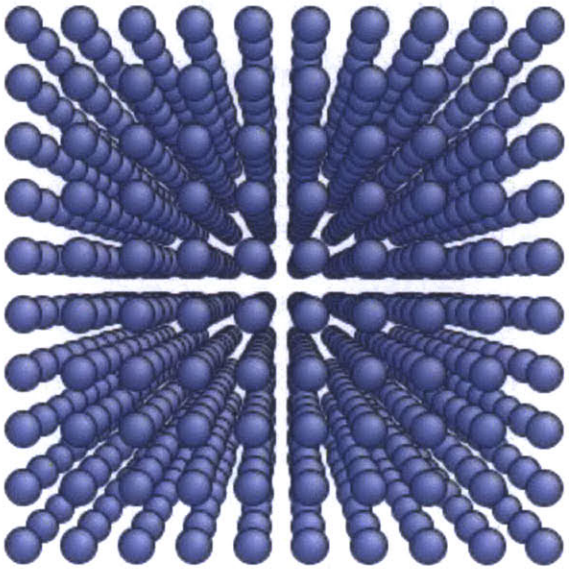

Figure 17. Atomic view of the test structure used.

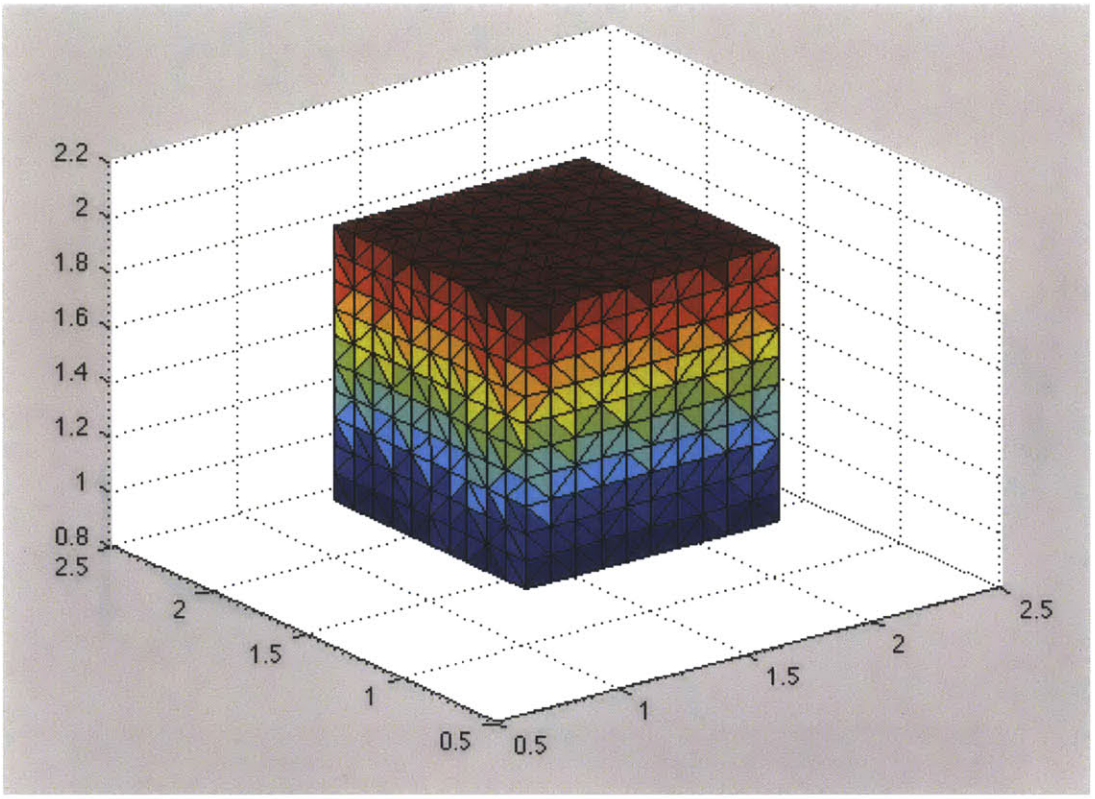

Figure 18. Mesh produced from the Dupuy and Rudd algorithm viewed in MATLAB. This mesh has 1200 triangular faces and 602 vertices. Plugging these values into Equation 5 yields a genus of zero.

The second simple test structure used was a simple torus. In order to create the torus test structure, points were placed on a cubic lattice and subject to a random displacement, as in the first cube test structure. Then, points outside of an inputted torus boundary were removed from the structure. For the test structure, a cubic lattice with lattice parameter 0.05 units and a total side length of 1 unit was used. The bounding torus had a ring radius, R_T, of 0.5 units and an axial radius, R_a, of 0.2 units. Using the Dupuy and Rudd algorithm, a surface mesh with 1067 vertices and 2134 faces was produced. Using these values, the calculated genus was found to be one, which matched the known value. Atomic views of the torus test structure and the mesh produced when using the Dupuy and Rudd algorithm are given in Figure 19.

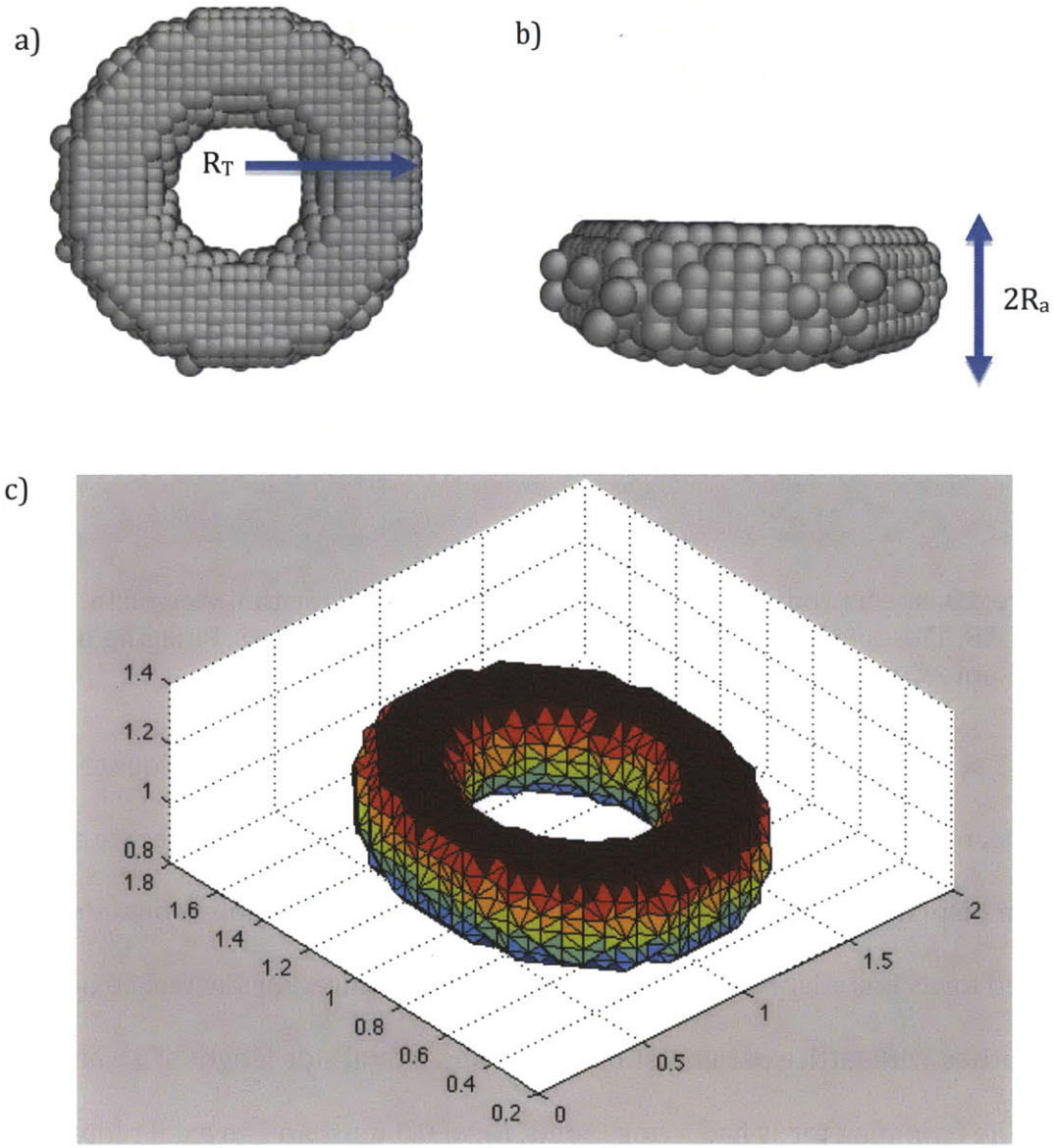

Figure 19. a-b) Two different atomic views of the torus structure used, as well as c) the mesh produced by the Dupuy and Rudd algorithm. In (a) and (b), what is meant by the radius R_T and R_a is clearly depicted.

The Delaunay triangulation method was also attempted for this test structure; however it failed to produce the correct results. A 3D mesh created using Delaunay triangulation is a volumetric mesh where no point in the point cloud being meshed is inside the sphere enclosing an element of the mesh. In order to create a surface mesh, the convex hull of this volumetric mesh was then taken. Since the convex hull of a surface is the envelope enclosing the surface, this method was unable to identify handles, such as that present in the torus. There may have been a way to create a Delaunay triangulation of the surface without using the convex hull method. Regardless, this method would have difficulty identifying which atoms are surface atoms, which made me abandon this meshing method in favor of the Dupuy and Rudd algorithm.

3.2. Small Test Structure

Before meshing the nanoporous gold structures generated by Kolluri et al., which have hundreds of thousands of atoms with many ligaments, a smaller test structure was first meshed. This was done in order to test the run time for a larger scale structure with many surface atoms, to see if any errors arose when meshing ligaments with irregular geometries, and to check the genus calculated from mesh attributes against a genus found from visual inspection. This smaller test structure was a porous copper sample with four ligaments and 10,000 atoms.

The structure was first meshed using the original Dupuy and Rudd algorithm. The mesh generated had 3129 vertices and 6326 faces. Both an atomic view of the structure and the generated mesh are depicted in Figure 22. Interestingly, the genus

for this surface mesh, calculated using Equation 5, is 18, which is different from the genus of the structure without periodic boundary conditions. From visual inspection, it is easy to see that the structure has a topological genus of three. This can be easily found by finding the maximum number of cuts one can make without separating the structure into multiple pieces. Typically, disparities between the calculated genus and the actual genus of a structure result from gaps or self-intersecting faces in the mesh. However, the generated mesh had not gaps or self-intersections.

The disparity between the calculated genus and the genus from visual inspection can be explained by the small sections of the structure near the boundaries that have small regions that are one atom thick. An example of such a section is shown in Figure 23a. It is important to note that there would be no regions with atomic thickness in the actual structure, because such regions would be at a very high energy and would quickly coarsen, either by the surface diffusion-based mechanism or the plasticity-based mechanism outlined in the introduction.Although these regions are actually connected to more matter at the opposite periodic boundary, the Dupuy and Rudd algorithm treats these regions as surface atoms. As such, it meshes both sides of these regions, resulting in a mesh where regions thin down to a single point. This causes a net increase in the topological genus.

To illustrate how a two-dimensional surface element would increase the topological genus, consider a square pyramid with one of the sides cut out, similar to Figure 23a. This shape is illustrated in Figure 23b. Such a surface would have six

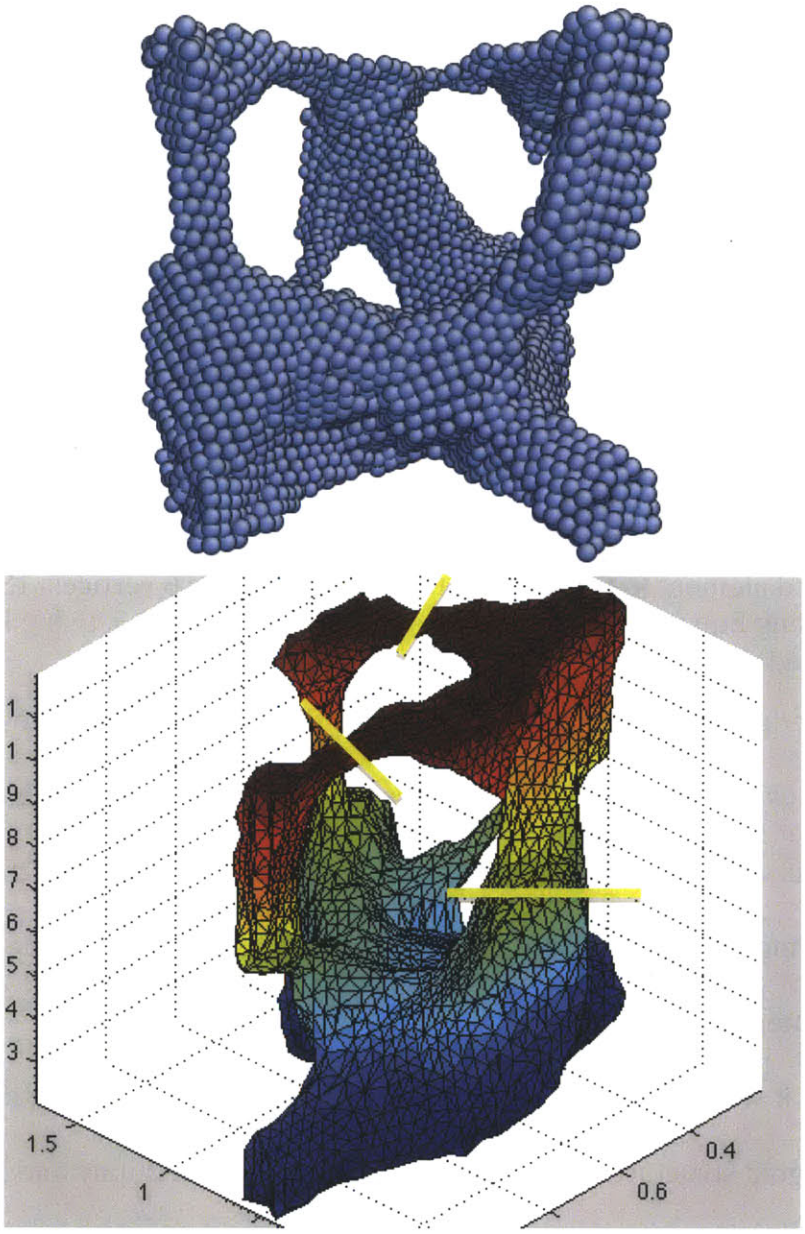

Figure 22. Atomic view of the small structure and the generated mesh. From a visual inspection, one can note that three cuts in the structure can be made without separating the structure into disparate pieces. Three possible cuts are indicated by the solid yellow lines.

a) b)

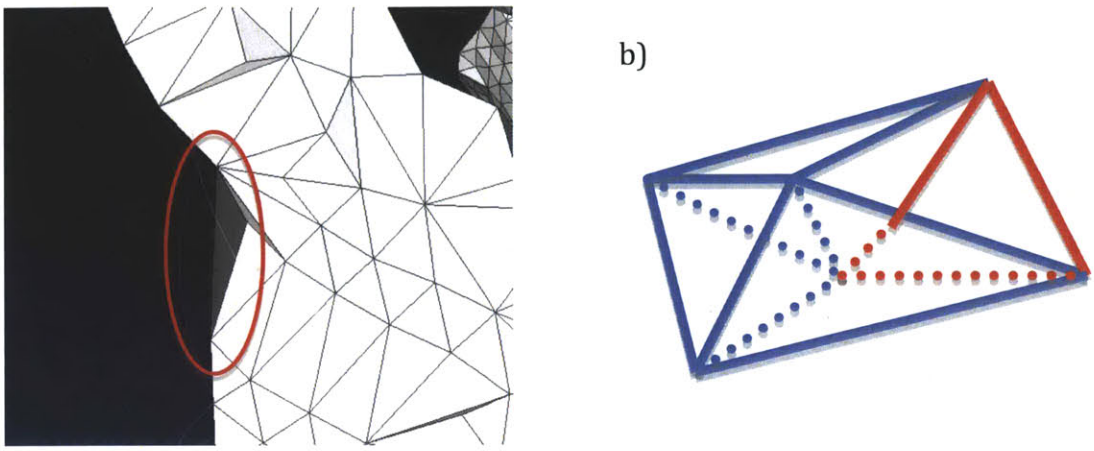

Figure 23. a) An example of a 2D surface element of the mesh, and b) a cartoon drawing of a surface with a 2D element. The circled dark element in (a) is 2D. The red bordered element in (b) is 2D. In (b), note that it has 6 vertices, 13 edges, and 10 faces. Using Equation 4, the calculated genus would be -0.5. Using Equation 5, the calculated genus would be 0.5.

vertice s, 13 edges, and 10 faces. There are two things to note from these values. First, the genus for the surface, calculated using Equation 4, is -0.5, which does not agree with the value of 0.5, calculated using Equation 5. Second, note that the genus calculated using Equation 5 is positive, which explains the higher value for the genus calculated using the generated mesh.

While it was previously known that the genus per unit volume for the nanoporous gold structures using a mesh generated by the Dupuy and Rudd algorithm would not be accurate, it was assumed that the calculated genus would be an underestimate, because the mesh would not account for ligaments that connect over periodic boundaries. However, meshing the results from the small structure mesh show that the computed genus for a mesh generated by the Dupuy and Rudd algorithm could also be higher than the actual genus, if there are regions near the boundary with atomic thickness.

4. CONCLUSIONS

After meshing several test structures and a small-scale nanoporous structure, it was found the algorithm proposed in the Dupuy and Rudd paper is not suitable for genus calculations for nanoporous metal structures with periodic boundary conditions. The algorithm does aptly find all surface atoms within a cell and create a high-quality mesh from those surface atoms, as evidenced by the successful meshing of the test structures and the small-scale nanoporous structure. However, the calculated genus per volume will be radically different from the true genus per volume of the structure. These differences are the result of regions with atomic thickness at the boundary and not accounting for the increased genus caused by ligaments connecting over the boundary.

In order to accurately mesh the nanoporous gold structures, an algorithm that accounts for periodic boundary conditions while meshing would be required. I currently have a version of a function that accounts for periodic boundary conditions, but the run-time is too long for these large-scale structures to produce results in a timely fashion. Future work on this project would certainly include improving the efficiency of this algorithm, in order to be able to produce results in a timely fashion. This would allow for the meshing of many nanoporous structures, which could then be used to study the time evolution of genus.

Other future work for this project would include further characterization of the surface of the nanoporous structures over time. It would be very interesting to examine the surface curvature of these structures, because surface curvature is a major driving force for surface diffusion in a material. It may also be interesting to quantify the surface area of the material over time, since the surface area of the

material of particular interest in catalytic applications. It would also be interesting to devise a way to find the number of pinch-off events that occur over time and connect this quantity with the changes observed in the characteristic genus.

5. ACKNOWLEDGEMENTS

I would like to thank Professor Demkowicz for his guidance throughout the research process and for providing me with a workspace. I would like to thank Dr. Kolluri for providing nanoporous gold structures for meshing. Lastly, I would like to thank everyone Demkowicz group, especially Guoqiang Xu, Richard Baumer, and Abishek Kashinath, for their help throughout the semester.

---

[i] H. Lechtman, *Sci. Am.* **250**, 56 (1984)
[ii] S.J. Fleming, Images of artifacts at the University of Pennsylvania Museum, <http://www.penn.museum/sites/applied_science/archaeometallurgy/sitio_conte_gold.html>
[iii] H.W. Pickering, *Corros. Sci.* **23**, 1107 (1983)
[iv] J. Erlebacher, M. Aziz, A. Karma, A. Dimitrov, K. Sieradzki, *Nature* **410**, 450 (2001)
[v] H.J. Jin, D. Kramer, Y. Ivanisenko, J. Weissmuller, *J. Adv. Eng. Mater.* **9**, 849 (2007)
[vi] J.C. Thorp, K. Sieradzki, L. Tang, P.A. Crozier, A. Misra, M. Nastasi, et al., *Appl. Phys. Lett.* **88**, 033110 (2006)
[vii] Z. Qi, C. Zhao, X. Wang, J. Lin, W. Shao, Z. Zhang, et al., *J. Phys. Chem.* C **113**, 6694 (2009)
[viii] D.E. Williams, R.C. Newman, Q. Song, R.G. Kelly, *Nature* **350**, 216 (1991)
[ix] R.C. Newman, K. Sieradzki, *Science* **263**, 1708 (1994)
[x] X. Lu, E. Bisehoff, R. Spolenak, T.J. Balk, *Scr. Mater.* **56**, 557 (2007)
[xi] R. Li, K. Sieradzki, *Phys. Rev. Lett.* **68**, 1168 (1992)
[xii] J. Erlebacher et al., *MRS Bull.* **34**, 561 (2009)
[xiii] X.Y. Lang et al., *Appl. Phys. Lett.* **94**, 213109 (2009)
[xiv] R. Wilson, *Chem Soc Rev* **37**, 2028 (2008)
[xv] K. Hu, D. Lan, X. Li, S. Zhang, *Anal Chem* **80**,9124 (2008)
[xvi] R.G. Mitsunori Hieda, M. Dixon, T. Daniel, D. Allara, M.H.W. Chang, *Appl. Phys. Lett.* **84**, 628 (2004)
[xvii] I. Dutta et al., *J. Phys. Chem. C* **114**, 16309 (2010)
[xviii] M. Shao et al., *J. Am. Chem. Soc.* **132**, 9253 (2010)
[xix] J. Snyder, T. Fujita, M.W. Chen, J. Erlebacher, *Nat. Mater.* **9**, 904 (2010)
[xx] Y. Ding, M. Chen, J. Erlebacher, *JACS* **126**, 6876 (2004)
[xxi] J. Biener, A. Wittstock, L.A. Zepeda-Ruiz, M. Biener, V. Zielasek, D. Kramer, et al., *Nat. Mater.* **8**, 47 (2009)

[xxii] A.M. Hodge et al., *Acta Mater.* **55**, 1343 (2006)
[xxiii] J.R. Greer, W.D. Nix, *Phys. Rev. B* **73**, 245410 (2006)
[xxiv] J. Biener, A.M. Hodge, A.V. Hamza, *Appl. Phys. Lett.* **87**, 121908 (2005)
[xxv] H. Rosner et al., *Adv. Eng. Mater.* **9,** 535 (2007)
[xxvi] S. Van Petegem et al., *Nano Lett.* **9**, 1158 (2009)
[xxvii] Y. Kwon, K. Thornton, P. Voorhees, *Phys. Rev. E* **75**, 021120 (2007)
[xxviii] T. Fujita, L.H. Qian, K. Inoke, J. Erlebacher, M.W. Chen, *Appl. Phys. Lett.* **92**, 251902 (2008)
[xxix] A.J. Forty, *Nature (London)* **282**, 597 (1979)
[xxx] C. Herring, *J. Appl. Phys.* **21**, 301 (1950)
[xxxi] S. Parida et al., *Phys. Rev. Lett.* **97**, 035504 (2006)
[xxxii] Y.C.K. Chen et al., *Appl. Phys. Lett.* **96**, 043122 (2010)
[xxxiii] J. Erlebacher et al., *Phys. Rev. Lett.* **106**, 225504 (2011)
[xxxiv] K. Kolluri, M. Demkowicz, *Acta Mater.* **59**, 7645 (2011)
[xxxv] M.S. Daw, M.I. Baskes, *Phys. Rev. Lett.* **50**, 1285 (1983)
[xxxvi] M.P Allen, "Introduction to Molecular Dynamics Simulation," Lecture Notes, <http://www2.fz-juelich.de/nic-series/volume23/allen.pdf>
[xxxvii] R. Mendoza et al., *Acta Mater.* **54**, 743 (2006)
[xxxviii] D.S. Richeson, *Euler's Gem*, Princeton University Press (2008)
[xxxix] L.M. Dupuy, R.E. Rudd, *Modeling Simul. Mater. Eng.* **14**, 229 (2006)